Chinese Chemical Letters 35 (2024) 109454

Contents lists available at ScienceDirect

Chinese Chemical Letters

journal homepage: www.elsevier.com/locate/cclet

Single-atom sites regulation by the second-shell doping for efficient electrochemical CO_2 reduction

Qian-Qian Tang[a,b], Li-Fang Feng[a,b], Zhi-Peng Li[a,b], Shi-Hao Wu[a,b], Long-Shuai Zhang[a,b,*], Qing Sun[a], Mei-Feng Wu[a,b], Jian-Ping Zou[a,b,*]

[a] Key Laboratory of Jiangxi Province for Persistent Pollutants Control and Resources Recycle, Nanchang Hangkong University, Nanchang 330063, China
[b] National-Local Joint Engineering Research Center of Heavy Metals Pollutants Control and Resource Utilization, Nanchang Hangkong University, Nanchang 330063, China

ARTICLE INFO

Article history:
Received 13 September 2023
Revised 16 December 2023
Accepted 25 December 2023
Available online 26 December 2023

Keywords:
Single-atom catalyst
Heteroatom-doping
Second shell
CO_2 electroreduction
Electronic structure regulation

ABSTRACT

Nitrogen-doped carbon loaded single-atom catalysts (SACs) are promising candidates for electrocatalytic conversion of CO_2 into high-valuable chemicals, and the modification of catalysts by heteroatom-doping strategy is an effective approach to enhance the CO_2 reduction performance. However, the large difference exists in atomic radius between nitrogen atoms and the doped heteroatoms may lead to the poor stability of active sites. In this study, we have synthesized a Ni single atom catalyst with S doping at the second-shell on the ultrathin carbon nanosheets support (Ni-N_4-SC) by solid-phase pyrolysis. The S atom in the second-shell contributes to the higher efficiency of CO_2 conversion at lower potentials while the Ni-N_4-SC can be more stable. The experimental results and theoretical calculations indicate that the S atom in second-shell breaks the uniform charge distribution and reduces the free energy of hydrogenation, which can increase the adsorption of CO_2, accelerate charge transfer, and reduce the reaction energy barrier. This work reveals the close relationship between the second-shell and the electrocatalytic activity of single atom sites, which also provides a new perspective to design efficient single atom catalysts.

Electrochemical conversion of carbon dioxide (CO_2) to value-added chemicals is a promising approach to develop carbon cycling and carbon neutrality [1–3]. Owing to the highly thermodynamic stability and slow dynamics of CO_2 reduction reaction (CO_2RR), constructing optimal catalysts is critical for efficient electrochemical CO_2RR [4–6]. Among the various CO_2RR catalysts, single-atom catalysts (SACs) have been considered as an excellent candidate because of their high atomic utilization, homogeneous active sites, and unique electronic structure [7–10]. Especially, for the nitrogen-doped carbon loaded SACs, in which the metal atom was immobilized by the coordination bonds to form the M-N_x (M: metal atom) structure, show high-loading, high-conductivity, and high-activity [11,12]. For example, the Fe-N_4 and Ni-N_4 sites SACs achieved high efficiency and selectivity for CO_2 to CO [13,14]. However, in the single-atom active sites with a M-N_x structure, the symmetry and strong electronegativity of adjacent N atoms reduce the CO_2 adsorption and increase the reaction energy barriers, leading to a great limitation for its CO_2RR activity at low potentials [15,16].

It has been suggested that replacing one or more N atoms with other heteroatoms in M-N_x can significantly modulate the electronic structure of active sites and change their local charge density [17–19]. The heterogeneous nonmetallic elements doping can alter the electronic structure of the M-N_x active sites by forming the N and other heteroatoms co-coordinated asymmetric M-N_xX_y structure (X: nonmetallic atom) [20–22]. For example, the N and S co-coordinated Ni single atom catalyst achieved low activation energy for the reduction of CO_2 [23]. However, the large difference exists in atomic radius between N and S atoms, and the weak interaction between metal and S also result in the poor stability of M-N_xS_y active sites [24,25]. The integration of heteroatoms (*i.e.*, P, O, B, and S) into carbon skeleton can not only improve the hydrophilicity of carbon materials but enhance the thermal stability [26,27]. Based on this, we propose the introduction of heteroatoms into the second-shell of M-N_x sites, which can not only greatly affect the electronic structure, but also avoid the influence of bond length and atomic radius on the stability of the M-N_x sites.

Herein, a Ni single atom catalyst with S doping in the second-shell of Ni-N_4 moiety (Ni-N_4-SC) by solid-phase pyrolysis was ob-

* Corresponding authors at: Key Laboratory of Jiangxi Province for Persistent Pollutants Control and Resources Recycle, Nanchang Hangkong University, Nanchang 330063, China.
E-mail addresses: l_s_zhang1990@163.com (L.-S. Zhang), zjp_112@126.com (J.-P. Zou).

https://doi.org/10.1016/j.cclet.2023.109454
1001-8417/

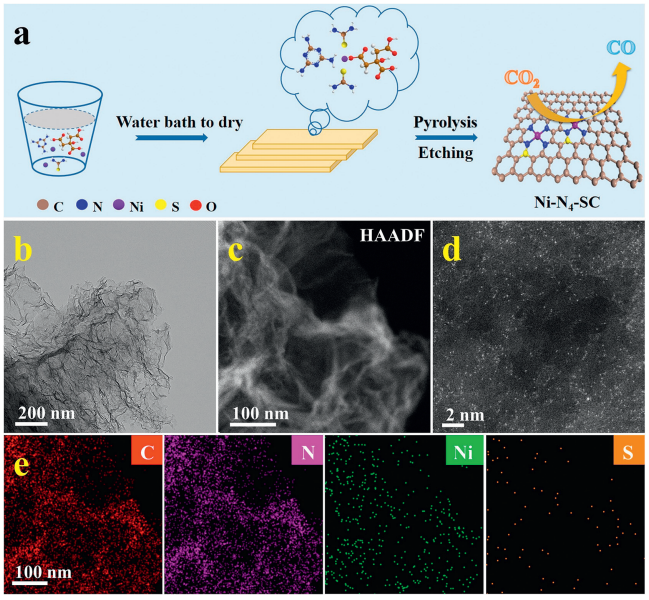

Fig. 1. (a) Synthesis schematic of the Ni-N_4-SC. (b) TEM, (c) HAADF-STEM, (d) AC-HAADF-STEM images, and (e) elemental mappings of the Ni-N_4-SC.

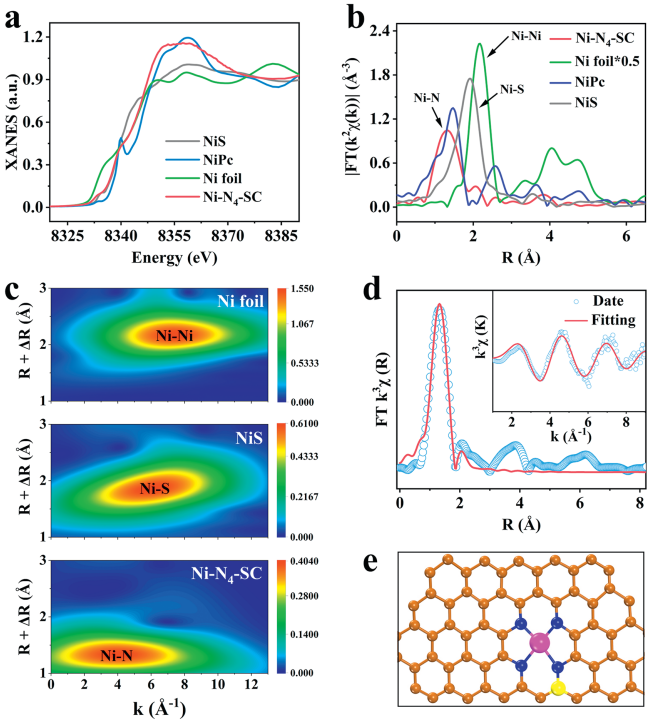

Fig. 2. (a) Ni K-edge XANES spectra, (b) Fourier transform of Ni K-edge EXAFS spectra, and (c) WT-EXAFS plots of Ni foil, NiS, and Ni-N_4-SC. (d) EXAFS fitting curve in R space, and (e) structure model of the Ni-N_4-SC.

tained. The Ni-N_4-SC presents high activity and stability of CO_2 electroreduction. DFT calculations show that the S atoms in the second-shell of Ni-N_4 significantly affect the highly symmetric structure of Ni-N_4 and make the Ni atom a more electron-rich state while reducing the activation free energy for the intermediates. This study provides a new standpoint for the design of highly efficient and more stable single atom active sites by introducing heteroatoms into the second-shell.

The synthesis schematic of Ni-N_4-SC is illustrated in Fig. 1a. During the high-temperature carbonization of the precursors, the melamine and thiourea provided N and S atoms into the carbon lattice by the released gasses [28,29]. Meanwhile, the Ni atoms were coordinated with N atoms. As shown in Fig. S1 (Supporting information), the XRD pattern of Ni-N_4-SC only shows two peaks at 26.2° and 44.0°, which belong to the (002) and (100) of graphite [30,31]. And there are no characteristic peaks attributed to the Ni species detected, indicating the absence of metallic Ni. As shown in Figs. 1b and c, the Ni-N_4-SC presents an ultrathin two-dimensional (2D) nanosheets structure with a thickness of approximately 7.5 nm as measured by AFM (Fig. S2 in Supporting information). In addition, no obvious clusters or nanoparticles are observed in Ni-N_4-SC (Figs. 1b and c, Figs. S3a and b in Supporting information), which is consistent with XRD results. As depicted in Fig. 1d, the AC-HAADF-STEM image shows that the Ni species are atomically dispersive (light spots). Furthermore, the energy dispersive X-ray spectroscopy (EDS) further demonstrates that Ni, N, and S are uniformly dispersed throughout the carbon support (Fig. 1e and Fig. S3c in Supporting information). The Ni single atom catalyst without S doping (Ni-N_4-C) was also successfully prepared (Fig. S4 in Supporting information). The mass fraction of Ni in Ni-N_4-SC is confirmed to be 6.97 wt% by inductively coupled plasma emission spectroscopy (ICP-OES, Table S1 in Supporting information). In addition, the contents of each element in Ni-N_4-C and Ni-N_4-SC were obtained by analyzing the X-ray photoelectron spectroscopy (XPS) data (Fig. S5a in Supporting information).

To further confirm the coordination environment and chemical state of Ni atoms in Ni-N_4-SC, X-ray absorption near edge structure (XANES) and extended X-ray absorption fine structure (EXAFS) were carried out. As shown in Ni K-edge XANES spectra (Fig. 2a), the absorption edge of Ni-N_4-SC is located much closer to that of NiS than that of Ni foil. Combined with the XPS results (Fig. S5b in Supporting information), it is shown that Ni atoms are in an oxidation state about +2 [12,32]. In addition, the Ni species in Ni-N_4-SC showed a more reductive state relative to Ni-N_4-C evidenced by the blueshift of binding energy at 0.54 eV, which may be induced by the neighboring S atoms [33]. As shown in Fig. 2b, the Ni-N_4-SC has only one peak located at 1.32 Å while Ni-Ni bond (2.18 Å) and Ni-S bond (1.93 Å) are not detected, which is consistent with the wavelet transform (WT) contour plots of samples (Fig. 2c). The similarity in the position of the maximum peak in Ni-N_4-SC and nickel phthalocyanine (NiPc) proves the presence of Ni-N bonds. Additionally, such characterization results could be supported by an XPS spectra analysis. As demonstrated in Fig. S5c (Supporting information), the high resolution N 1s XPS spectrum of Ni-N_4-SC revealed Ni-N as well as other nitrogen species, while Ni-S bonding species are ruled out by the S 2p XPS spectrum of Ni-N_4-SC (Fig. S5d in Supporting information), which prove again that the Ni is coordinated with N atoms rather than S atoms. In addition, based on the EXAFS fitting data provided in Table S2 (Supporting information), it can be seen that no signals from the Ni-S bond were fitted to the Ni-N_4-SC. Therefore, the Ni atoms in Ni-N_4-SC are atomically dispersion and directly coordinated by N atoms. As can be seen in Fig. 2d, the experimental results are in good agreement with the fitted model, confirming that the Ni atoms are coordinated with four N atoms and S is doped in the second shell of Ni-N_4. The corresponding structural model is displayed in Fig. 2e.

The electrocatalytic CO_2RR activities of samples were tested in a three-electrode system with 0.5 mol/L $KHCO_3$ as the electrolyte. Compared with saturated Ar atmosphere, the Ni-N_4-SC presents a significant increase in cathodic current density and a positive shift in onset potential with saturated CO_2 (Fig. 3a), indicating that the Ni-N_4-SC tends to reduce CO_2 rather than H^+ [19,25]. The electrochemical CO_2 reduction activities of samples were evaluated by linear scanning voltammetry (LSV), which shows that the Ni-N_4-SC presents superior electrochemical activity compared with the sam-

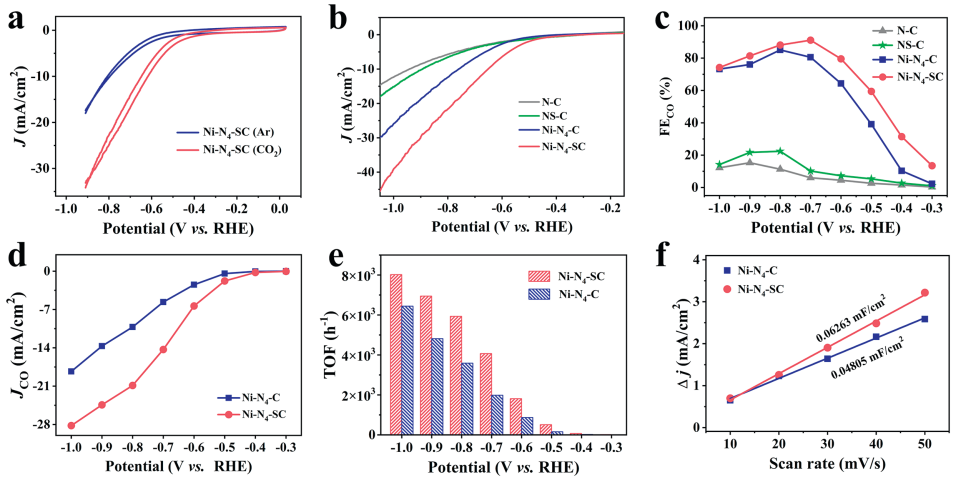

Fig. 3. (a) CV curves of the Ni-N_4-SC under different atmosphere. (b) LSV curves of samples. (c) FE_{CO} of samples. (d) CO partial current density (J_{co}) at different potentials. (e) TOF of Ni-N_4-C and Ni-N_4-SC at different potentials. (f) Charging current density differences plotted against scan rates.

ples without Ni and/or S (Fig. 3b) [14,34]. The liquid and gaseous products were analyzed using ^{1}H NMR spectroscopy and gas chromatography (GC), respectively. As illustrated in Fig. S6 (Supporting information), there are no liquid products detected in both Ni-N_4-C and Ni-N_4-SC systems. The Faraday efficiency of CO product (FE_{CO}) for each catalyst at different potentials shows that the single Ni atoms are the catalytic active sites, and that S doping inhibits the HER side-reaction to enhance CO_2 reduction activity, particularly at relatively low potentials (Fig. 3c and Fig. S7 in Supporting information). In addition, the electrocatalytic reduction tests under different atmospheres show that the product of CO was from CO_2 (Fig. S8 in Supporting information). As shown in Fig. 3d, the Ni-N_4-SC shows a higher CO partial current density of -28.21 mA/cm^2 at -1.0 V *vs.* RHE than Ni-N_4-C. The intrinsic activities of the samples were evaluated through the calculated turnover of frequency (TOF) of the CO product. As depicted in Fig. 3e, the TOF values of Ni-N_4-SC are higher than Ni-N_4-C at electrode potentials between -0.4 V and -1.0 V *vs.* RHE, which also indirectly proves that the S in the second-shell of Ni-N_4-SC is indeed favorable for boosting CO_2RR activity [23,35]. In Fig. 3f, the Ni-N_4-SC exhibits a larger electrochemical surface area, estimated by the double-layer capacitance (CdI) method (Fig. S9 in Supporting information), indicating that Ni-N_4-SC has more active sites than Ni-N_4-C [7,36]. The FE_{CO} maintains up to 95% over 24 h under a constant voltage at -0.7 V *vs.* RHE (Fig. S10 in Supporting information), which shows the stability of Ni-N_4-SC.

To further explain the origin of the superior CO_2RR catalytic performance of Ni-N_4-SC, DFT calculations were carried out. The adsorption of CO_2 on the surface of the catalyst is a prerequisite for the CO_2RR [5]. As shown in Fig. 4a, the adsorption energy of the Ni-N_4-SC for CO_2 molecule is more negative than that of Ni-N_4-C, confirming that the presence of S in the second-shell helps Ni-N_4-SC possess a stronger capacity of CO_2 adsorption. Furthermore, the differential charge density of Ni-N_4-C and Ni-N_4-SC prove that the S in the second-shell of Ni-N_4-SC breaks the uniform charge distribution around the Ni atoms and makes the Ni atom a more electron-rich state (Fig. 4b), which facilitates the transfer of electrons to the adsorbed CO_2 molecule [37]. As shown in Fig. 4c, the hydrogenation process of the adsorbed CO_2 molecules is the rate-limiting step overall reaction. When the S atom is introduced into the second-shell of the active site, the free energies of the CO_2 reduction with rate-limiting step decrease from 1.954 eV of Ni-N_4-C to 0.876 eV of Ni-N_4-SC, which further demonstrates that the S can promote the conversion of CO_2 to *COOH. According to the above

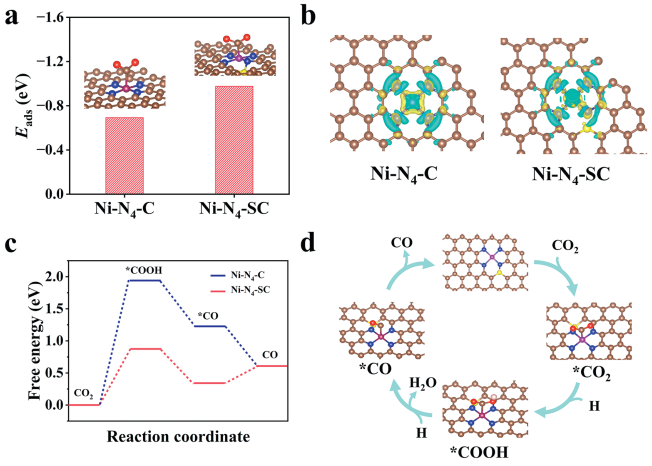

Fig. 4. (a) Adsorption energies of CO_2, (b) charge density difference map, and (c) free energies diagram for the CO_2 conversion to CO of the Ni-N_4-C and Ni-N_4-SC. (d) The proposed reaction paths of Ni-N_4-SC for electroreduction CO_2 to CO.

results, the S in the second-shell can accelerate electron migration to the Ni active site and reduce the reaction energy barrier in the process of CO_2 reduction. The reaction path of Ni-N_4-SC for CO_2 electroreduction is proposed as demonstrated in Fig. 4d. Based on these experimental results and DFT calculations, it is known that the Ni single atoms act as the active site and the introduction of S in the second-shell of Ni-N_4 is the key factor to increase the electrocatalytic CO_2RR activity and selectivity for CO production.

In summary, a Ni single-atom electrocatalyst with S doping at the second-shell of the Ni sites on the ultrathin carbon nanosheets support was successfully synthesized for CO_2RR. The S atoms in the second-shell of Ni sites help the Ni-N_4-SC better improve the electrocatalytic CO_2 reduction and CO selectivity. Experimental results and DFT calculations show that the S in the second-shell can accelerate electron migration and reduce the reaction energy barriers of CO_2 reduction, thus boosting CO_2 reduction activity. Simultaneously, the S atoms in the second-shell can also avoid the instability caused by its large atomic radius. This study provides a new viewpoint for the exquisite design of single atom active sites with adjustable electronic structure and good stability by doping heteroatoms in the second-shell of the M-N_x sites.

Declaration of competing interest

The authors declare that they have no known competing financial interests or personal relationships that could have appeared to influence the work reported in this paper.

Acknowledgments

We gratefully acknowledge the financial support of the National Natural Science Foundation of China (Nos. 52100186, 52170082, 51938007 and 52063024) and the Jiangxi Provincial Natural Science Foundation (Nos. 20225BCJ23003 and 20212ACB203008).

Supplementary materials

Supplementary material associated with this article can be found, in the online version, at doi:10.1016/j.cclet.2023.109454.

References

[1] Z.Q. Li, B. Sun, D.F. Xiao, et al., Angew. Chem. Int. Ed. 62 (2023) e202217569.
[2] J.P. Zou, Y. Chen, S.S. Shan, et al., Water Res. 150 (2019) 330–339.
[3] M.F. Wu, Q.H. Ruan, H.X. Jiang, et al., J. Mater. Chem. A 10 (2022) 25463–25470.
[4] H. Wang, H.Y. Chuai, X.Y. Chen, et al., ACS Appl. Mater. Interfaces 15 (2023) 1376–1383.
[5] M. Zhu, L.S. Zhang, S.S. Liu, et al., Chin. Chem. Lett. 31 (2020) 1961–1965.
[6] Y.X. Tuo, W.L. Liu, Q. Lu, et al., Chem. Eng. J. 464 (2023) 142510.
[7] M.H. Han, D.J. Kim, S.K. Kim, et al., Adv. Energy Mater. 12 (2022) 2201843.
[8] L.Z. Liu, M.T. Li, F. Chen, H.W. Huang, Small Struct. 4 (2023) 2200188.
[9] Q.Q. Tang, L.S. Zhang, J.P. Zou, Chinese J. Struc. Chem. 41 (2022) 1–2.
[10] J.X. Peng, W.J. Yang, Z.H. Jia, L. Jiao, H.L. Jiang, Nano Res. 15 (2022) 10063–10069.
[11] D.M. Koshy, S.C. Chen, D.U. Lee, Angew. Chem. Int. Ed. 59 (2020) 4043–4050.
[12] S. Hu, P.Z. Qiao, X.L. Yi, Angew. Chem. Int. Ed. 62 (2023) e202304585.
[13] X.G. Li, S.B. Xi, L.B. Sun, et al., Adv. Sci. 7 (2020) 2001545.
[14] X.G. Li, W.T. Bi, M.L. Chen, et al., J. Am. Chem. Soc. 139 (2017) 14889–14892.
[15] H.B. Yang, S.F. Hung, S. Liu, et al., Nat. Energy 3 (2018) 140–147.
[16] J. Leverett, L.L. Gong, K. Iputera, et al., ACS Nano 15 (2021) 12006–12018.
[17] X.H. Jiang, L.S. Zhang, H.Y. Liu, et al., Angew. Chem. Int. Ed. 59 (2020) 23112–23116.
[18] C.J. Chen, X.F. Sun, X.P. Yan, et al., Angew. Chem. Int. Ed. 59 (2020) 11123–11129.
[19] P.Z. Chen, T.P. Zhou, L.L. Xing, et al., Angew. Chem. Int. Ed. 56 (2017) 610–614.
[20] Q.H. Li, W.X. Chen, H. Xiao, et al., Adv. Mater. 30 (2018) 1800588.
[21] S. Lu, Y. Zhang, M.F. Mady, et al., ChemSusChem 15 (2022) e202200870.
[22] M.B. Ma, F.H. Lia, Q. Tang, Nanoscale 13 (2021) 19133–19143.
[23] X.Y. Zhao, S.H. Huang, Z.Y. Chen, et al., Carbon 178 (2021) 488–496.
[24] F.P. Pan, B.Y. Li, W. Deng, et al., Appl. Catal. B: Environ. 252 (2019) 240–249.
[25] H.Y. Tan, S.C. Lin, J.L. Wang, et al., ACS Appl. Mater. Interfaces 13 (2021) 52134–52143.
[26] Q.Q. Lu, K. Eid, W.P. Li, Nanomaterials 12 (2022) 2379.
[27] H.N. Che, X. Gao, J. Chen, et al., Angew. Chem. Int. Ed. 60 (2021) 25546–25550.
[28] M. Jourshabani, Z. Shariatinia, A. Badiei, et al., Langmuir 33 (2017) 7062–7078.
[29] H.P. Yang, Y. Wu, G.D. Li, et al., J. Am. Chem. Soc. 141 (2019) 12717–12723.
[30] A.X. Guan, Z. Chen, Y.L. Quan, et al., ACS Energy Lett. 5 (2020) 1044–1053.
[31] W. Hua, H. Sun, L. Lin, et al., Chem. Eng. J. 446 (2022) 137296.
[32] L.S. Zhang, X.H. Jiang, Z.A. Zhong, et al., Angew. Chem. Int. Ed. 60 (2021) 21751–21755.
[33] S.Y. Chen, X.Q. Li, C.W. Kao, et al., Angew. Chem. Int. Ed. 61 (2022) e202206233.
[34] X.T. Wang, T. Ouyang, L. Wang, et al., Angew. Chem. Int. Ed. 58 (2019) 13291–13296.
[35] Y.M. Cai, J.J. Fu, Y. Zhou, et al., Nat. Commun. 12 (2021) 586.
[36] T. Ouyang, Y.Q. Ye, C.Y. Wu, K. Xiao, Z.Q. Liu, Angew. Chem. Int. Ed. 58 (2019) 4923–4928.
[37] P.F. Hou, Y.H. Huang, F. Ma, et al., Appl. Surf. Sci. 619 (2023) 156747.